Chapter 3
Resolution of Multicomponent Systems and Speciation

3.1 Introduction

In the previous chapter, methodologies for identifying individual species in works of art have been presented for cases where only one (or one main) electroactive component is present. Such electrochemical methods, however, can be extended to cases in which several electroactive species contribute to the observed electrochemical response. Resolution of multicomponent systems, considered here as a possibility for simultaneously identifying different electroactive compounds in the sample, can be achieved by applying different methodologies. These can, in principle, be divided into: (a) "electrochemical" methodologies, based on the variation of electrochemical parameters and handling of electrochemical data, and, (b) "chemical" methodologies, based on the selective choice of chemical inputs (pH variation, complexing electrolytes) for improving the electrochemical discrimination of the components of the sample. Within "electrochemical" methodologies, we can distinguish: (i) the use of pattern recognition criteria by taking shape-dependent parameters for individual electrochemical signals; (ii) application of bi-parametric classification schemes; and (iii) the application of multivariate chemometric methods. This chapter will be devoted to describing these approaches in order to identify different components in samples from works of art and archaeological artifacts. Obviously, electrochemical methods can be complemented with nonelectrochemical techniques to obtain analytical information demanded for conservators and restorers [169–172].

It is important to note that the application of electrochemical methods to the analysis of samples of art objects and archaeological artifacts allows much more than only simple identification of certain constituents: advanced methods of speciation may provide information about constituents that are only slightly differing in their composition, or for which there are only slight differences in the matrices in which the components are embedded. Further, redox speciation—and in the case of solid samples, phase speciation—can be used to derive information on production processes or corrosion (deterioration) of the components in the time that passed since their formation. The second part of this chapter is devoted to illustrating the capabilities of advanced speciation strategies.

A. Doménech-Carbó et al., *Electrochemical Methods in Archaeometry, Conservation and Restoration*, Monographs in Electrochemistry,
DOI 10.1007/978-3-540-92868-3_3, © Springer-Verlag Berlin Heidelberg 2009

3.2 Analysis of Single Multicomponent Systems

In several cases, samples from works of art contain different electroactive species that provide separated signals. This is frequent in paint samples where different pigments—and eventually, alteration products—exist. In general, such components occur as microparticles highly diluted in a nonelectroactive matrix so that independent voltammetric responses are, in principle, recorded. This is the case for a sample of medieval glaze from Manises (Valencia, Spain), the square wave voltammogram of which is depicted in Fig. 3.1. Here, cathodic peaks at +0.70, −0.08, −0.45, and −0.56 V appear. The first two peaks correspond, respectively, to the reduction of Mn(IV) and Sn(IV), while the third and fourth peaks can be ascribed to the reduction of Sn(II) and Pb(II) to the corresponding metals [173]. This response provides information on the composition of the glaze and denotes the presence of manganese as a coloring agent in that sample [128].

Figure 3.2 shows the square wave voltammetric response for: (a) azurite, (b) tenorite (CuO), and (c) a sample from the frescoes in the ceiling vault of the *Sant Joan del Mercat* church in Valencia (Spain)—all attached to PIGEs and immersed into 0.50 M acetate buffer. These frescoes, painted by Antonio Acisclo Palomino in 1707 suffered considerable damage by fire during the Spanish civil war in 1936. As can be seen in Fig. 3.3, a substantial part of the paintings was entirely destroyed, while most of the surviving areas presented significant chromatic changes [133, 172, 174].

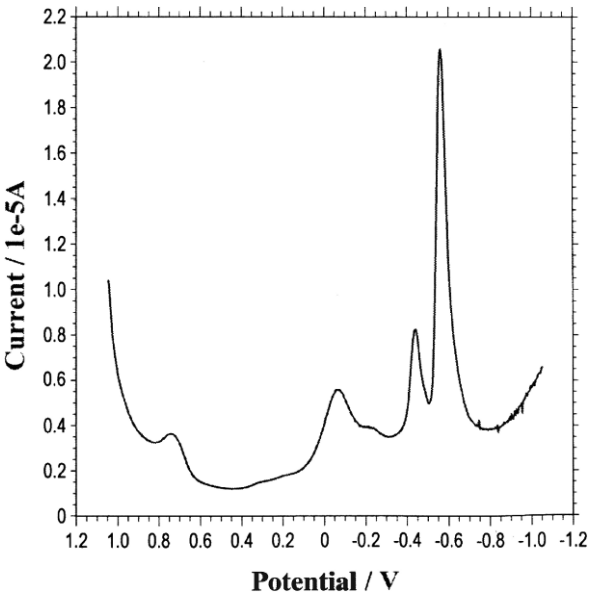

Fig. 3.1 Square wave voltammogram for a sample of mediaeval glaze from Manises (Valencia, Spain). Electrolyte 0.50 M sodium acetate buffer, pH 4.85. Potential step increment 4 mV; square wave amplitude 25 mV; frequency 5 Hz

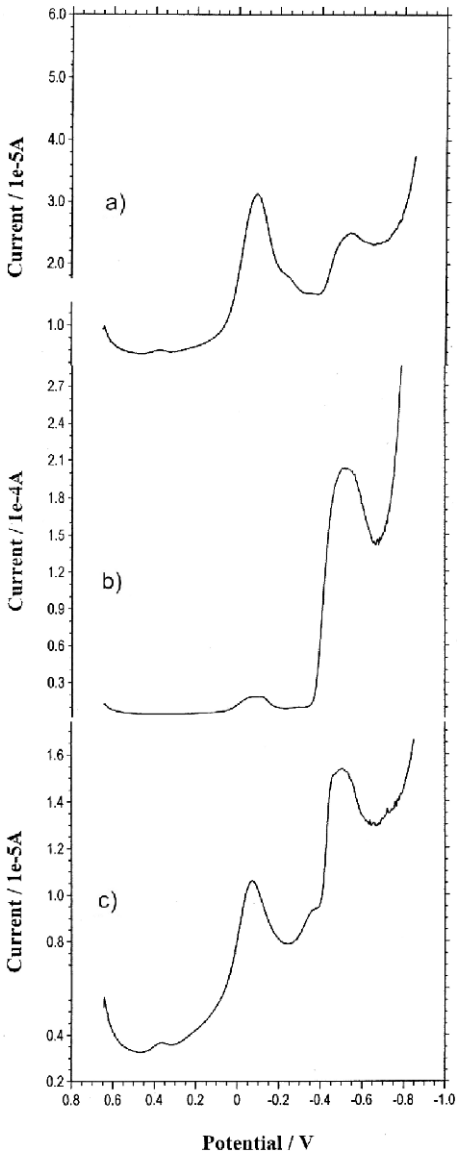

Fig. 3.2 Square wave voltammograms of: (**a**) azurite, (**b**) CuO, and (**c**) a sample from the *Sant Joan del Mercat* church in Valencia (Spain), attached to PIGEs and immersed in 0.50 M sodium acetate buffer (pH 4.85). Potential scan initiated at +0.65 V in the negative direction. Potential step increment 4 mV; square wave amplitude 25 mV; frequency 5 Hz [133]

SQWVs of "green" paint layers confirmed the presence of azurite and azurite plus smalt mixtures accompanied by tenorite (CuO) in several samples as a result of thermal decomposition of azurite. Since azurite decomposition starts at 345°C with a loss of CO_2 and water, slowly yielding CuO which is then converted to cuprite (Cu_2 O) at 840°C [175], and since no traces of this last mineral were detected in any sample, one can conclude that the effective temperature reached by the pigments in such samples ranged from 350 to 840°C.

Fig. 3.3 Image of a portion (area ca. 1 m^2) of the damaged Palomino's frescoes in the vault of the *Sant Joan del Mercat* church in Valencia (Spain) [133]

3.3 Criteria for Pattern Recognition

In most cases, electrochemical data consists of a series of well-separated peaks due to the reduction/oxidation of different electroactive species existing in the sample. Identification of the component responsible for each peak can, in principle, be derived from the peak potential, in a given electrolyte, under fixed electrochemical conditions. This parameter, however, depends (in the case of solid materials) on the shape and size distribution (i.e., in a wide meaning, its granulometric characteristics) of the particles of electroactive compound. Apart from this, matrix effects (complexing ions existing in the sample) can also modify the observed voltammetric response, which, in turn, is also frequently shifted by an uncompensated ohmic drop in the cell and capacitive effects. As a result, it is desirable to use additional parameters defining diagnostic criteria for shape recognition. On the basis of criteria used by Sybrandt and Perone [176], different electrochemical parameters can be used for pattern recognition in cyclic voltammetric curves. Among others, one can mention:

(a) Onset potentials defined by prolonging the almost-linear regions in the ascendant (E_{onset}) and descending (E'_{onset}) branches of the reduction (or oxidation) peak to intersect the potential axis. It should be noted, however, that these onset potentials have no strictly defined meaning.
(b) Half-peak width $W_{1/2}$, defined as the potential separation between the points of the peak whose current is just one half of the peak current.
(c) The semi-half-peak widths, defined as the differences between the peak potential and the potentials of the above points in the increasing $(\Delta E_{p/2})_1$ and decreasing $(\Delta E_{p/2})_2$ portions of the voltammetric peak. The quotient $r = (\Delta E_{p/2})_1/(\Delta E_{p/2})_2$ between these two parameters defines a symmetry factor for the voltammetric peak.

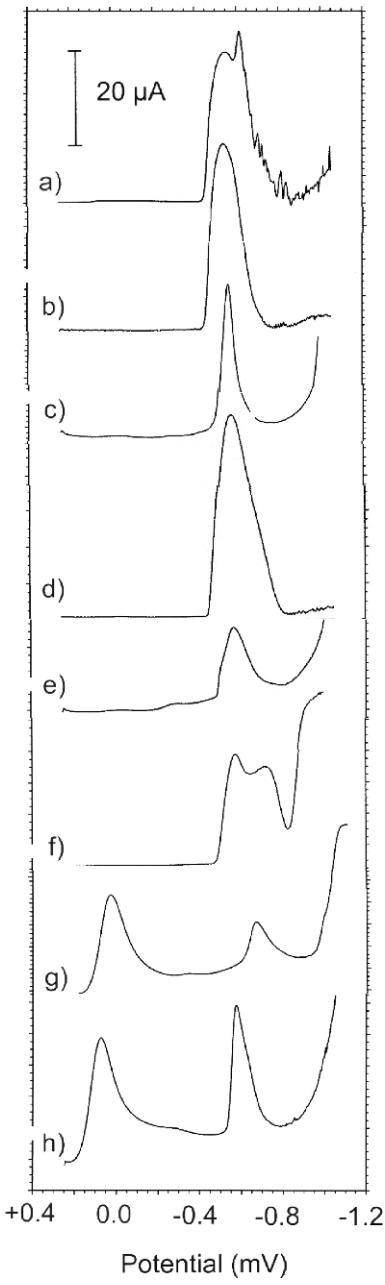

Fig. 3.4 Square wave voltammograms of microsamples of: (**a**) litharge, (**b**) massicot, (**c**) *Naples yellow*, (**d**) *lead white*, (**e**) *tin-lead yellow*, (**f**) minium, (**g**) *chrome orange*, and (**h**) *chrome yellow* attached to parafin-impregnated graphite electrodes. Electrolyte: 0.50 M sodium acetate buffer, pH 4.85. Potential step increment 4 mV; square wave amplitude 25 mV; frequency 15 Hz [177]

Table 3.1 Diagnostic criteria for characterizing lead pigments via voltammetry of microparticles using deposits of the pristine pigments on paraffin-impregnated graphite electrodes. Data from square-wave voltammograms at a potential step increment of 4 mV, square-wave amplitude of 25 mV, and frequency of 15 Hz. All potentials refer to AgCl (3M NaCl)/Ag. Electrolyte, 0.50 M acetate buffer, pH 4.85

Pigment	E_p (mV)	$W_{1/2}$ (mV)	$(\Delta E_{p/2})_1$ (mV)	$(\Delta E_{p/2})_2$ (mV)	r
Chrome Orange	−605	115	35	80	0.44
Chrome Yellow	−570	85	25	60	0.42
Lead White	−555	180	65	115	0.56
Litharge	−540	160	65	95	0.68
Massicot	−540	145	60	85	0.70
Minium	−545	155	50	105	0.48
Naples Yellow	−540	65	30	35	0.86
Tin-lead Yellow	−570	135	60	75	0.80

(d) Separation between the potentials for which current is 3/4 and 1/4 of the peak current in the main reduction wave, $E_{3/4} - E_{1/4}$. This parameter, representing the "mean" inclination of the current/potential curve, is of interest for characterizing voltammetric processes displaying highly overlapping peaks [176].

The convenience of using multiparametric pattern recognition criteria can be illustrated by the problem of identifying lead pigments in pictorial samples [126]. Figure 3.4 compares square-wave voltammograms for: (a) litharge, (b) massicot, (c) Naples yellow, (d) lead white, (e) tin-lead yellow, (f) minium, (g) chrome orange, and (h) chrome yellow attached to paraffin-impregnated graphite electrodes immersed in acetate buffer. Lead pigments exhibit a prominent reduction peak at about −0.55 V corresponding to the reduction of the corresponding lead compound into lead metal. For instance, for litharge or massicot,

$$PbO_s + 2H^+{}_{aq} + 2e^- \rightarrow Pb_s + H_2O \tag{3.1}$$

Only chrome yellow and chrome orange (lead chromates) exhibit an additional peak at +0.45 V, attributable to the reduction of chromate ions:

$$PbCrO_{4s} + 8H^+{}_{aq} + 3e^- \rightarrow Cr^{3+}{}_{aq} + Pb^{2+}{}_{aq} + 4H_2O \tag{3.2}$$

As can be seen in Fig. 3.4, peak potentials for lead-centered reduction processes are similar, so pigment identification can be improved by considering a series of parameters, as summarized in Table 3.1.

3.4 Bi-Parametric Data Analysis

Combination of selected pairs of variables in two-dimensional (2D) diagrams enables a separation between different electroactive materials. This can be seen in Fig. 3.5, where a representation of $(E_{3/4} - E_{1/4})$ vs. $(E'_{onset} - E_{onset})$ measured in

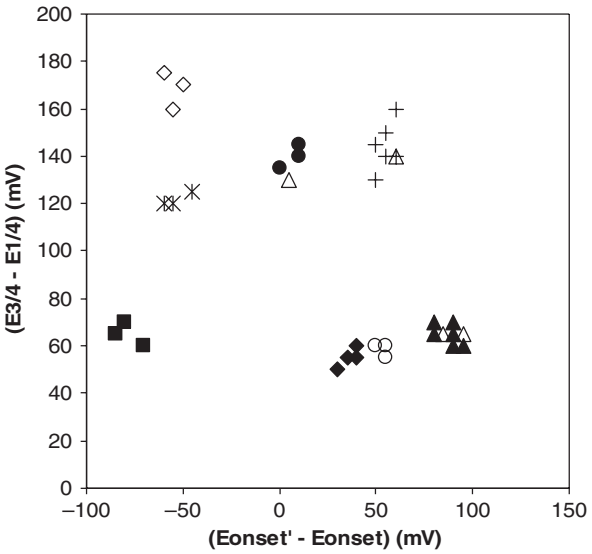

Fig. 3.5 Representation of $(E_{3/4} - E_{1/4})$ vs. $(E'_{onset} - E_{onset})$ for lead pigments, model paint specimens, and real samples. Data from CVs recorded in the AFM cell for nanosamples attached to a graphite plate. Electrolyte: 0.50 M acetate buffer. Potential scan rate 100 mV/s. *Solid rhombs* = chrome orange; *solid squares* = chrome yellow; *solid triangles* = lead white; *rohmbs* = litharge; *stars* = massicot; *solid circles* = minium; *crosses* = Naples yellow; *circles* = tin-lead yellow. Real samples for different paint specimens (see details in ref. [126]) are marked by *triangles*

cyclic voltammograms for lead pigments, model paint specimens, and real samples attached to a graphite plate in an electrochemical atomic force microscopy cell immersed in acetate buffer is depicted [126]. Here, the inherent capabilities of electrochemical AFM are used for recording the voltammetric response of nanosamples of pictorial specimens.

Although the presence of binding media and other materials accompanying pigment in samples influences voltammetric signals, under appropriate selection of the electrochemical parameters and operating conditions [126], voltammetric responses become pigment-characteristic and fall in clearly separated regions of the 2D diagram.

In favorable cases, detailed analysis of electrochemical parameters can provide information on the composition of complex systems such as pigments plus binding media in paint samples. In general, voltammetric profiles of pigments can be modified to any extent by the presence of other materials in the sample—binding media in particular. As it is well-known, pigments are accompanied in such samples by bindings and other materials—namely, proteinaceous materials and drying oils, either alone or mixed together.

This can be seen in Fig. 3.6, where square-wave voltammograms for synthetic pictorial specimens contain recommended dosages [177] of lead white, plus: (a) casein and (b) sunflower oil. As depicted in Fig. 3.3, the response of the pristine pigment consisted of a unique peak at −0.56 V. The pictorial specimens

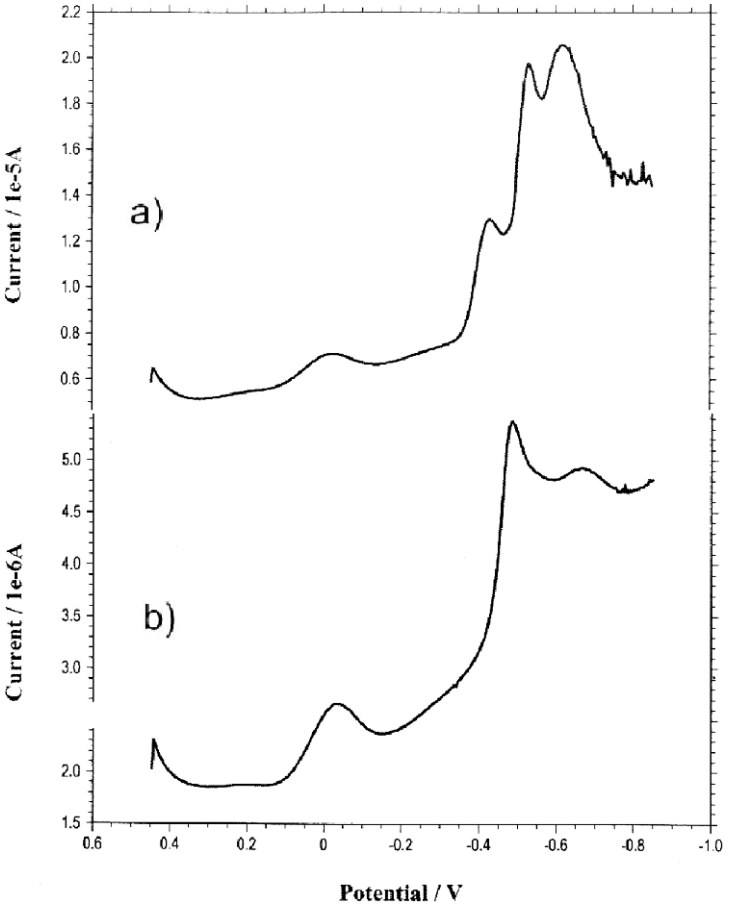

Fig. 3.6 SQWVs for synthetic specimens containing lead white plus (**a**) casein and (**b**) sunflower oil, immersed into 0.50 M sodium acetate buffer, pH 4.85. Potential step increment 4 mV; square wave amplitude 25 mV; frequency 15 Hz [177]

provided significantly binder-dependent profiles. Thus, casein peaks at −0.43, −0.54, and −0.62V appear, while square-wave voltammograms provided a sharp peak at −0.48 V for oil-containing specimens followed by a shoulder at ca. −0.65 V.

The above voltammetric responses can be rationalized by assuming that the response of the grains of pristine pigments is superimposed to that of the ionomeric layer containing lead-binder compounds [178, 179]. For lead carbonate, this can be represented as [126, 177]

$$PbCO_{3s} + 2H^{+}{}_{aq} + \{binder\} \rightarrow \{Pb^{2+} - binder\} + H_2O + CO_2 \qquad (3.3)$$

$$\{Pb^{2+} - binder\} + 2H^{+}{}_{aq} + 2xe^{-} \rightarrow xPb_s + (1-x)Pb^{2+}{}_{aq} + \{2H^{+} - binder\} \qquad (3.4)$$

$$Pb^{2+}{}_{aq} + 2e^- \rightarrow Pb_s \tag{3.5}$$

In these equations, {} represents species confined in the ionomeric layer surrounding the grains of pigment. In the case of proteinaceous binders, Pb^{2+} ions are probably coordinated to any extent to donor sites of the binder, so that Eq. 3.3 should be replaced by

$$Pb^{2+} - \{binder\} + 2e^- \rightarrow Pb_s + \{binder\} \tag{3.6}$$

Additionally, the ionomeric layer can form a barrier for charge diffusion surrounding the particles of pigment. As a result, the rate of the overall electrochemical process described by Eqs. 3.3, 3.4 and 3.5 is modified. Our data suggest that the peak at ca. -0.45 V is attributable to the reduction of free (Eq. 3.5) or binder-coordinated (Eq. 3.6) Pb^{2+} ions, while peaks at ca. -0.65 V must correspond to the reduction scheme described by Eqs. 3.3 and 3.4.

Figure 3.7 shows a 2D diagram corresponding to the plot of $(E_{onset} - E_p)$ vs. $W_{1/2}$ for the peak at -0.45 V for lead white plus proteinaceous binders (squares), lead white plus oils (triangles), minium plus proteinaceous binders (solid squares), and Naples yellow plus oils (solid triangles). In this diagram, one can see that data points for pigments plus proteinaceous binder samples fall in a region separated from that where data points for pigment plus oil binders are grouped.

Characterization of the binding media can be improved using plots of the potential separation between the peaks at -0.45 and -0.65 V, ΔE_p, vs. $W_{1/2}$ for a peak at -0.45 V. As shown in Fig. 3.8, data points for two proteinaceous binders, casein and bovine gelatin, applied to different pigments (lead white, minium, Naples yellow)

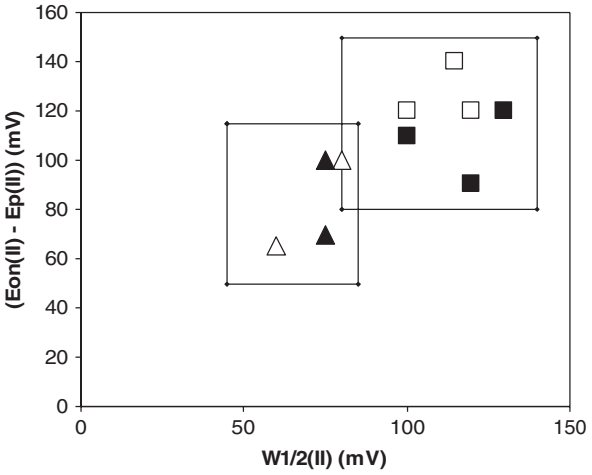

Fig. 3.7 Plot of $(E_{onset} - E_p)$ vs. $W_{1/2}$ for the peak at -0.45 V for different lead pigment plus binder specimens: lead white plus proteinaceous binders (*squares*), minium plus proteinaceous binders (*solid squares*), lead white plus oils (*triangles*), and Naples yellow plus oils (*solid triangles*). From square-wave voltammetric data using the conditions described in the caption of Fig. 3.3

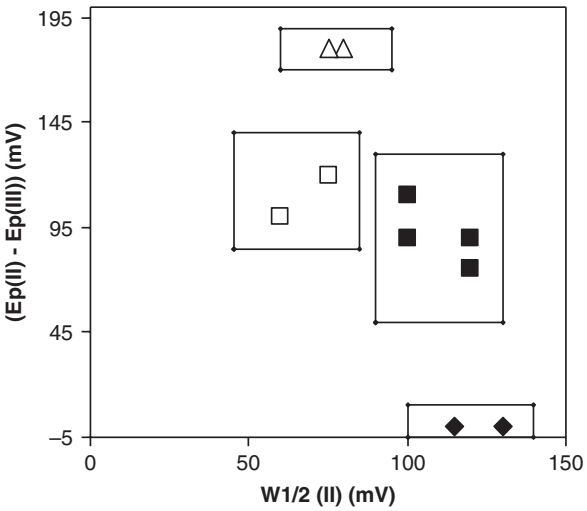

Fig. 3.8 Plot of the potential separation between the peaks at −0.45 and −0.65 V, ΔE_p vs. $W_{1/2}$ for peak at −0.45 V for different lead pigment plus binder specimens: *solid squares* = casein or bovine gelatin plus lead white or minium = *squares*: lead white and Naples yellow plus poppy oil; *triangles* = sunflower plus lead white and Naples yellow; *solid rhombs* = egg plus lead white and minium. From square-wave voltammetric data using the conditions from Fig. 3.3

fall in a narrow central region of the diagram. Data points for sunflower oil, poppy oil, and egg are in turn grouped in other, well-separated regions of the diagram.

In several instances, data analysis is complicated by the possible coexistence of different electroactive products in the sample having a similar electrochemical response. A typical case is provided by copper pigments and their alteration products in paint layers or metallic artifacts submitted to deterioration processes. Thus, Fig. 3.9a–d shows the square wave voltammograms for two typical pigments—azurite (a) and verdigris (c)—and two typical products of alteration of copper and bronze artifacts—cuprite (b), and atacamite (d)—all in contact with phosphate buffer. This last one is one of the crystalline forms of copper trihydroxychloride, which is a product of the alteration of pigments and copper pieces and eventually can also be used as a pigment [180].

In all these cases, a main reduction peak appears ca. −0.10 V so that a direct discrimination between the different species is uneasy. The situation in real samples is even more complicated because, as reviewed by Scott [181] and Tennenth [182], the alteration of bronze and copper artifacts produces (depending on the weathering conditions) different products, mainly cuprite and different minerals of the atacamite group (atacamite, paratacamite, clinoatacamite, botallakrite), accompanied by nantokite and ocasionally other rare minerals such as calumetite $(Cu(OH,Cl)_2 \cdot 2H_2O)$, anthonyte $(Cu(OH,Cl)_2 \cdot 3H_2O)$, and connellite $(Cu_{19}(SO_4)Cl_{14}(OH)_{32} \cdot 3H_2O)$ [181]. Another frequent product of alteration in bronze disease, nantokite (CuCl), exhibits a clearly discernable response consisting of a reduction peak at −0.36 V as shown in Fig. 3.10.

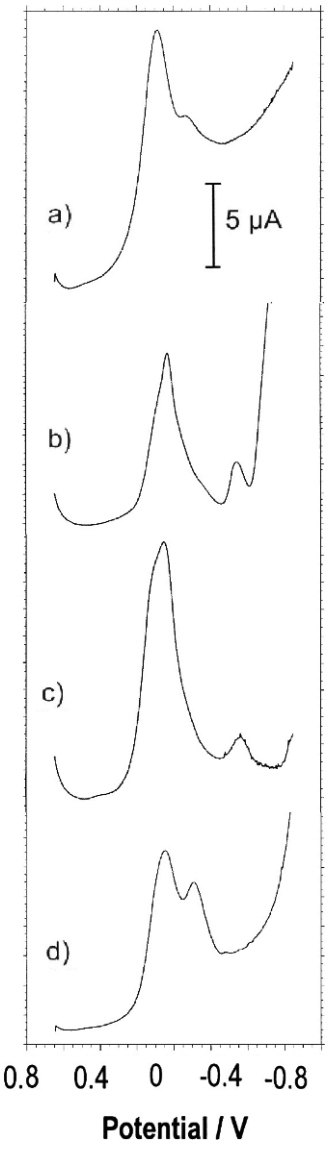

Fig. 3.9 SQWVs for (**a**) azurite, (**b**) cuprite, (**c**) verdigris, and (**d**) atacamite, in contact with 0.50 M potassium phosphate buffer, pH 7.4. Potential scan initiated at +0.45 mV in the negative direction. Potential step increment 4 mV; square wave amplitude 15 mV; frequency 2 Hz [133]

For solving mixtures of copper products, parameters derived from Tafel analysis of voltammetric curves were used [127, 133, 183]. The use of this formalism requires: (i) that electrochemical processes for individual analytes can be taken as independent, and (ii) strong overlapping of voltammetric curves. Both conditions apply in our studied samples because these systems can be taken as constituted by separated micro- or nanograins of different solid compounds. Tafel analysis is based on the assumption that the rising portion of voltammetric curves can, in general, be

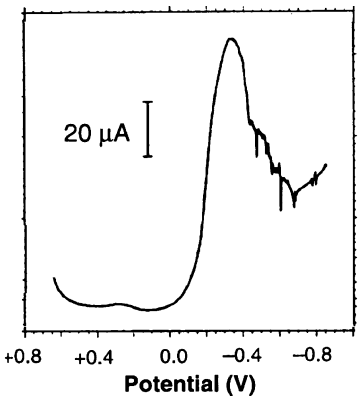

Fig. 3.10 Square-wave voltammogram of nantokite (CuCl) attached to PIGE in contact with 0.50 M potassium phosphate buffer, pH 7.0. Potential scan initiated at +650 mV in the negative direction. Potential step increment 4 mV; square wave amplitude 25 mV; frequency 5 Hz. Adapted from [183]

approached by an exponential dependence of the current on the applied potential regardless of the electrochemical mechanism. This is strictly valid for irreversible charge transfer processes involving species in solution phases, for which the current at the foot of the voltammetric peak satisfies [79, 80]

$$\mathrm{i} = \mathrm{Gn}(\alpha \mathrm{n_a})^{1/2} \mathrm{ckD} \exp\left[-\frac{\alpha \mathrm{n_a F(E - E_i)}}{\mathrm{RT}}\right] \tag{3.7}$$

In this equation, αn_a represents the product of the coefficient of electron transfer (α) by the number of electrons ($\mathrm{n_a}$) involved in the rate-determining step, n the total number of electrons involved in the electrochemical reaction, k the heterogeneous electrochemical rate constant at the zero potential, D the coefficient of diffusion of the electroactive species, and c the concentration of the same in the bulk of the solution. The initial potential is E_i and G represents a numerical constant. This equation predicts a linear variation of the logarithm of the current, $\ln i$, on the applied potential, E, which can easily be compared with experimental current-potential curves in linear potential scan and cyclic voltammetries. This type of dependence between current and potential does not apply to electron transfer processes with coupled chemical reactions [186]. In several cases, however, linear $\ln i$ vs. E plots can be approached in the rising portion of voltammetric curves for the solid-state electron transfer processes involving species immobilized on the electrode surface [131, 187–191], reductive/oxidative dissolution of metallic deposits [79], and reductive/oxidative dissolution of insulating compounds [147, 148]. Thus, linear potential scan voltammograms for surface-confined electroactive species verify [79]

$$i = \frac{n^2 F^2 v A \Gamma (b_{ox}/b_{rd}) \exp\left[-\frac{nF(E-E^{o\prime})}{RT}\right]}{RT\left[1 + (b_{ox}/b_{rd}) \exp\left[-\frac{nF(E-E^{o\prime})}{RT}\right]\right]^2} \tag{3.8}$$

In this equation, the b_{ox}/b_{rd} ratio represents the relative adsorption strengths of the oxidized and reduced species. For an irreversible process [79],

$$i = \mathrm{nFAk}\Gamma \exp\left[-\frac{\alpha \mathrm{n_a F(E - E^{o\prime})}}{\mathrm{RT}}\right] \exp\left[\frac{\mathrm{kRT}}{\alpha \mathrm{n_a Fv}} \exp\left[-\frac{\alpha \mathrm{n_a F(E - E^{o\prime})}}{\mathrm{RT}}\right]\right] \tag{3.9}$$

Equations 3.8 and 3.9 tend to a linear dependence of $\ln i$ on E for the limiting case when $\mathrm{E} \gg \mathrm{E^{o\prime}}$; i.e., at the beginning of the voltammetric peak.

Extension of this treatment to pulse techniques can, in principle, be made for several cases. In the case of square-wave voltammetry, theoretical current-potential curves for reversible electron transfer between species in solution are given by [184, 185]

$$\Delta i = \frac{nFAc\sqrt{Df}}{\sqrt{\pi}} \sum_{m=1}^{j} \frac{(-1)^j (Q_m - 2Q_{m-1} + Q_{m-2})}{(\delta + j - m)^{1/2}} \tag{3.10}$$

Where

$$Q_j = \frac{\exp(E_j - E^{o\prime})(nF/RT)}{1 + \exp(E_j - E^{o\prime})(nF/RT)} \tag{3.11}$$

In these equations, E_j represents the electrode potential during the jth half period, δ the fraction of the square-wave half period at which the current is measured, f is the square-wave frequency (equal to the inverse of the square-wave period), and the other symbols have their customary meaning. As long as the square-wave amplitude, E_{SW}, is lower than $0.5RT/nF$—a condition easily accomplished under the usual experimental conditions—the differential sum of the currents flowing during the anodic and cathodic half cycles can be represented by an expression such as [184]

$$\Delta i = H \frac{\exp(E - E^{o\prime})(nF/RT)}{[1 + \exp(E - E^{o\prime})(nF/RT)]^2} \tag{3.12}$$

Here, H represents an electrochemical constant.

Equation 3.12 again reduces to a Tafel linear $\ln i$ on E dependence in the foot of the voltammetric peak, a situation that applies with reasonable approximation for square-wave voltammograms of surface-confined species [79, 131].

Assuming that solid-state electrochemical processes involved in our voltammetry of microparticles analysis satisfy Tafel dependence between current and potential at the rising portion of voltammetric curves, the current can be approached by the expression

$$\mathrm{i} \approx \mathrm{q_o k} \exp\left(-\frac{\alpha \mathrm{n_a F}}{\mathrm{RT}} \mathrm{E}\right) \tag{3.13}$$

where q_o represents the total charge involved in the complete reaction of the electroactive solid. In the following section, it will be assumed that this kind of relationship is applicable not only to linear potential scan techniques, but also to pulse techniques, but also to pulse ones, in particular to square wave voltammetry, merely by inserting a numerical 'electrochemical' constant.

Equation 3.13 predicts a linear dependence of $\ln i$ on E whose slope depends on the coefficient αn_a, while the ordinate at the origin depends on the electrochemical rate constant and the net amount of depolarizer deposited on the electrode. Accordingly, both the slope and the ordinate at the origin of Tafel plots become phase-dependent [133, 183]. Since the quantity of depolarizer varies from one

experiment to another, it is convenient to use normalized currents. For this purpose, one introduces the expression for the peak current for a linear scan voltammetric current:

$$i_p = B\left(\frac{\alpha n_a F}{RT}\right) v q_o \tag{3.14}$$

With B being an electrochemical coefficient of the response characteristic of the electrochemical process, the electrode area, and v being the potential scan rate, combining Eqs. 3.13 and 3.14 obtains

$$\ln(\mathrm{i}/\mathrm{i_p}) = \ln\left(\frac{\mathrm{kRT}}{\mathrm{H}\alpha\mathrm{n_a F}}\right) - \frac{\alpha\mathrm{n_a F}}{\mathrm{RT}}\mathrm{E} \tag{3.15}$$

Here, both the Tafel slope ($\mathrm{SL} = \alpha\mathrm{n_a F/RT}$) and the ordinate at the origin ($\mathrm{OO} = \ln(\mathrm{kRT/B}\alpha\mathrm{n_a F})$) become characteristic of the solid, but are independent on the amount of analyte deposited on the electrode.

For a material containing a mixture of microparticles of two electroactive analytes that display highly overlapped voltammetric peaks, the currents at the beginning of the common voltammetric wave can be taken as additive, assuming that there is no significant interaction between the compounds. Accordingly, one can write

$$i \approx q_{oX} k_X \exp\left(-\frac{\alpha_X n_{aX} F E}{RT}\right) + q_{oY} k_Y \exp\left(-\frac{\alpha_Y n_{aY} F E}{RT}\right) \tag{3.16}$$

If $\alpha_j n_{aj} FE/RT << 1 (j = X, Y)$, one can use the approximation $e^{-z} \approx 1 - z$, so that Eq. 3.15 reduces to:

$$i \approx (q_{oX} k_X + q_{oY} k_Y) \exp\left[-\frac{(q_{oX} k_X \alpha_X n_{aX} + q_{oY} k_Y \alpha_Y n_{aY})(FE/RT)}{q_{oX} k_X + q_{oY} k_Y}\right] \tag{3.17}$$

Assuming as before that voltammetric peaks for X and Y are strongly overlapped, a unique peak will be recorded, and the peak potential can be expressed as:

$$i_p \approx B_X\left(\frac{\alpha_X n_{aX} F}{RT}\right) v q_{oX} + B_Y\left(\frac{\alpha_Y n_{aY} F}{RT}\right) v q_{oY} \tag{3.18}$$

Thus the i/i_p ratio will be given by the approximate expression:

$$\frac{i}{i_p} \approx \frac{(q_{oX} k_X + q_{oY} k_Y) RT}{(B_X \alpha_X n_{aX} q_{oX} + B_Y \alpha_Y n_{aY} q_{oY}) nFv} \exp\left[-\frac{(q_{oX} k_X \alpha_X n_{aX} + q_{oY} k_Y \alpha_Y n_{aY})(FE/RT)}{q_{oX} k_X + q_{oY} k_Y}\right] \tag{3.19}$$

This equation again fits to a linear dependence of $\ln i$ on E. This means that the sample containing a mixture of X plus Y should give a linear Tafel plot. Remarkably, both the slope and the ordinate at the origin of that representation should be intermediate between those obtained for the X and Y components separately (Eq. 3.15).

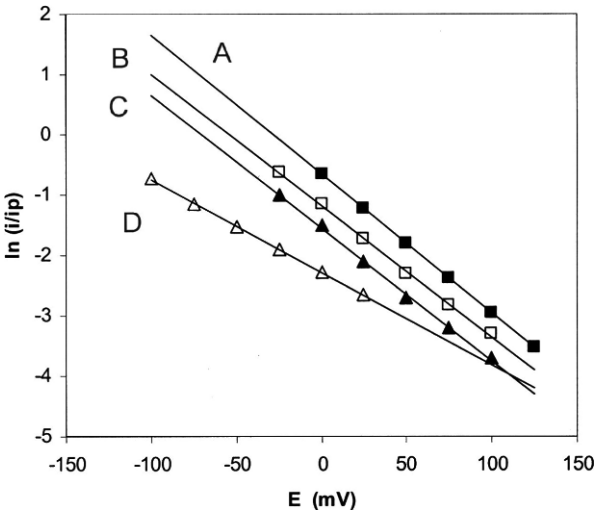

Fig. 3.11 Tafel plots for verdigris (**A**), atacamite (**B**), paratacamite (**C**), and cuprite (**D**) from linear scan voltammograms at sample-modified, paraffin-impregnated graphite electrodes immersed in 0.50 M potassium phosphate buffer (pH 7.0). Potential scan rate 50 mV/s

Typical Tafel plots for different copper materials are shown in Fig. 3.11. In all cases, an excellent linearity was obtained for $\ln(i/i_p)$ on E representations in terms of the correlation coefficient for linear fitting. Similar results were obtained for binary or ternary mixtures of such materials where highly overlapping peaks were recorded, both using linear potential scan and square-wave voltammetries.

This similarity makes it difficult to use pattern recognition criteria described in the precedent section because the involved parameters are not additive for mixtures of compounds, so that Tafel analysis of the rising portion of voltammetric curves offers a plausible alternative for resolution of mixtures. This is prompted by the fact that the values of *SL* and *OO* fell in well-separated regions in two dimensional diagrams, as shown in Fig. 3.12.

An example of the application of Tafel analysis is provided by samples taken for a bronze *montefortino* helmet from the Cabriel river valley (Kelin and Ikalesken period) in the Valencian region of Requena, dated back to the Second Iron Age (see Fig. 3.13). Upon attachment to paraffin-impregnated graphite electrodes immersed in 0.50 M phosphate buffer, voltammetric signals such as depicted in Fig. 3.14 were found [183].

According to the previous treatment, linear Tafel plots of $\ln(i/i_p)$ on E were obtained for samples providing from different regions of the helmet. As can be seen in Fig. 3.15, 2D diagrams using Tafel slope (*SL*) and Tafel ordinates at the origin (*OO*) yield a distribution of samples in three groups: one formed by cuprite (CI-11), one formed by atacamite (CI-4, CI-6, CI-9), and one formed by a mixture of cuprite plus atacamite (C-12).

A similar situation was found in the previously described frescoes of the vault of the *Sant Joan del Mercat* church in Valencia (Spain). In several regions of the vault, the attribution to this painter was uncertain because it was documented

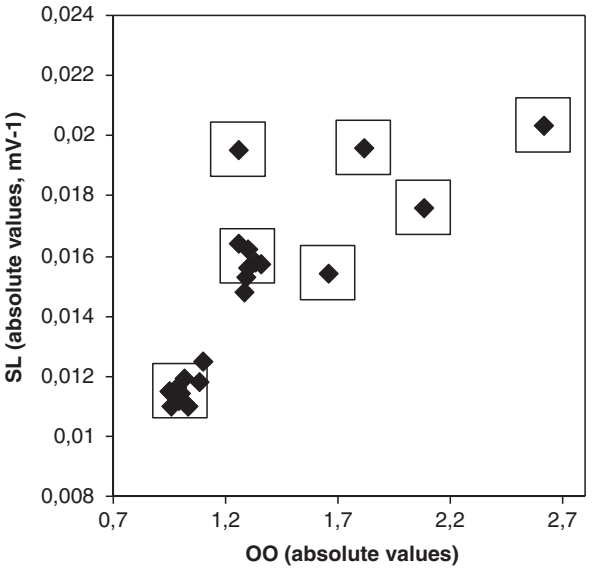

Fig. 3.12 Tafel *SL* vs. *OO* diagram for the most common copper pigments and copper alteration products. From SQWVs of specimen-modified paraffin-impregnated graphite electrodes immersed into 0.50 M phosphate buffer, pH 7.4. Potential scan initiated at +0.45 mV in the negative direction. Potential step increment 4 mV; square wave amplitude 15 mV; frequency 2 Hz

Fig. 3.13 Montefortino helmet from the Cabriel river valley (Kelin and Ikalesken period) in the Valencian region of Requena, dating back to the Second Iron Age [183]

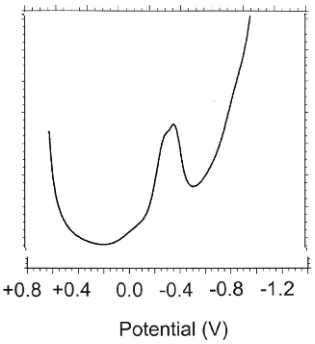

Fig. 3.14 Square-wave voltammograms of PIGEs modified with sample CI-12 from a bronze *montefortino* helmet from the Cabriel river valley (Kelin and Ikalesken period) in the Valencian region of Requena, dating back to the Second Iron Age. Electrolyte: 0.50 M potassium phosphate buffer, pH 7.0. Potential scan initiated at +650 mV in the negative direction. Potential step increment 4 mV; square wave amplitude 25 mV; frequency 5 Hz

that, in such regions of the vault, painter Vicente Guilló Barceló (1645–1698) started to execute a prior frescoes that were partially maintained despite the fact that Antonio Palomino was the painter in charge of the painting of the complete vault.

SEM/EDX analysis indicated that copper, frequently accompanied by cobalt pigments, was present in the samples from such frescoes. Analysis of voltammetric curves indicated that azurite or malachite, eventually accompanied by smalt, were the original pigments, and were accompanied (as previously described) by tenorite

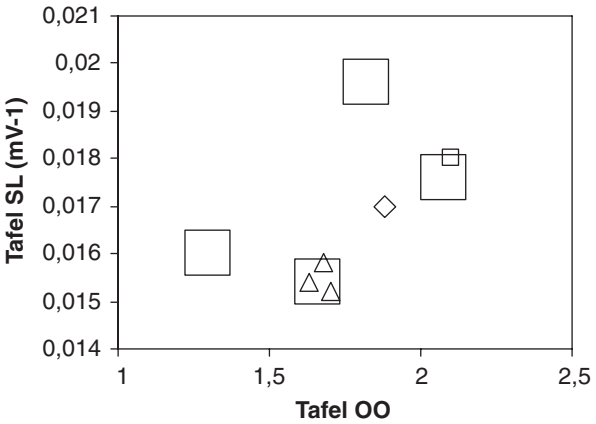

Fig. 3.15 Two-dimensional (2D) Tafel diagram corresponding samples CI-11 (*square*), CI-4, CI-6, CI-9 (*triangles*), and CI-12 (*rhomb*) from a bronze *montefortino* helmet from the Cabriel river valley (Kelin and Ikalesken period) in the Valencian region of Requena, dating back to the Second Iron Age. From SQWV data of sample-modified graphite electrodes in contact with 0.50 M phosphate buffer. Potential scan initiated at +0.65 V in the negative direction. Potential step increment 4 mV; square wave amplitude 25 mV; frequency 5 Hz. Adapted from [183]

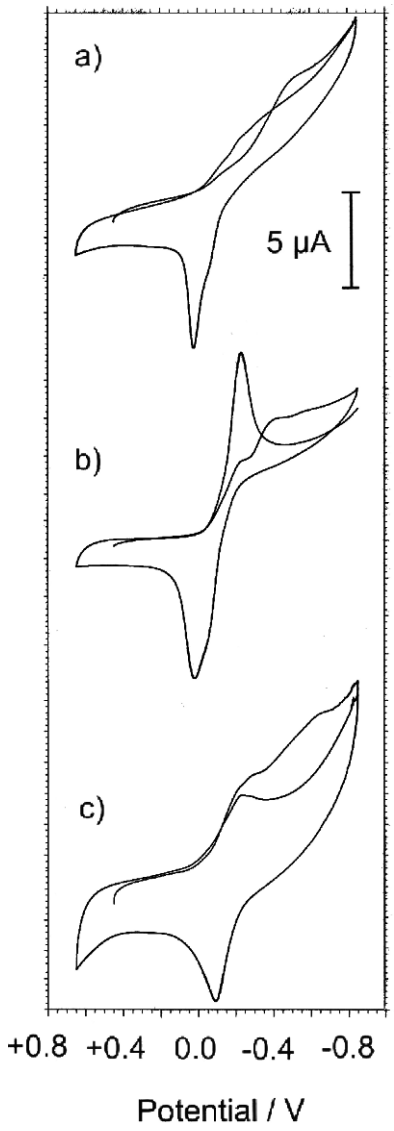

Fig. 3.16 CVs of PIGEs modified with (**a**) azurite, (**b**) malachite, and (**c**) smalt in contact (all Kremer pigments) immersed into 0.50 M potassium phosphate buffer of pH 7.4. Potential scan rate 50 mV/s [133]

in the zones exhibiting gunfire damage. Figure 3.16 shows the cyclic voltammetric responses of: (a) azurite, (b) malachite, and (c) smalt in contact with a phosphate buffer. In all cases, the reduction occurs at potentials ca. -0.10 V, leading to the corresponding metal deposit subsequently reduced via typical stripping processes at potentials ca. $+0.05$ V. As previously noted, analysis of stripping curves enables a clear distinction between copper and cobalt, thus indicating possible copper plus cobalt mixtures, as commented in Chap. 2 (see Fig. 2.10).

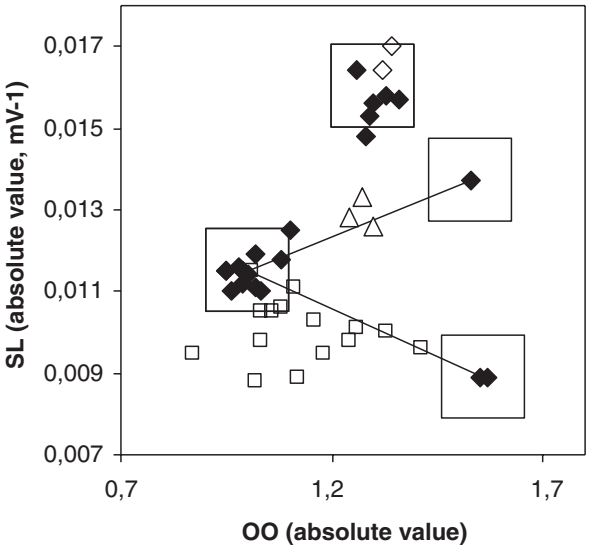

Fig. 3.17 A 2D Tafel slope vs. Tafel ordinate at the origin diagram for samples from the *Sant Joan del Mercat* church. From SQWVs at specimen-modified PIGEs immersed in 0.50 M phosphate buffer, pH 7.4 initiated at +0.65 V in the negative direction. Potential step increment 4 mV; square-wave amplitude 20 mV; frequency 5 Hz. *Solid figures* correspond to blanks of azurite, malachite, smalt, and smalt heated at 600°C. *Empty figures* correspond to samples provided from lightly altered regions of the vault (*squares*), strongly altered regions (*triangles*), and regions of the frescoes whose attribution to Palomino was uncertain (*rhombs*) [133]

In view of the close vicinity of the responses of these pigments, Tafel analysis was used for analyzing samples from the *Sant Joan del Mercat* church. The results are shown in Fig. 3.17, where samples are grouped into three types: those extracted from lightly and highly altered (blackened) areas of the vault in regions whose attribution to Palomino was clear, and those extracted from areas of the vault whose attribution to Palomino was in question. Blank specimens from commercial azurite, malachite, and smalt pigments, and those submitted to heating in a furnace at temperatures between 200 and 600°C were used. Interestingly, the heating of azurite and malachite specimens produced tenorite with no significant alteration in the Tafel parameters of surviving azurite or malachite signals. In contrast, heated specimens of smalt produced a significant shift in Tafel parameters [133].

As can be seen in Fig. 3.17, samples attributed to Palomino are divided into two regions between azurite and unheated smalt, and azurite and heated smalt—clearly denoting that Palomino used mixtures of both pigments in his paintings. Remarkably, the two samples from an uncertain author areas fell within the region of malachite. These results clearly suggest that these samples should be attributed to Vicente Guilló rather than to Palomino [133].

3.5 Multivariate Methods

Multivariate chemometric methods have claimed considerable attention in the last few decades because of their inherent capacity for resolving multicomponent, complex systems. Applications of multivariate methods in different electrochemical techniques have been recently reported by several authors [192–194].

An example of the application of these methods in the electrochemical field is the identification of earth pigments in paint layers. "Earths" are iron-based pigments composed by iron oxides and silicates. On the basis of their hue, iron earths can be divided into ochres (yellow), earths (red), siennas, umbers and green earths. On the basis of their mineralogy, earth pigments can be divided into clay-like yellow earths, calcium sulphate-based earths, umbers, and iron silicates. The most abundant clay-like earths results from lateritic weathering of mafic rocks, that are mainly composed by Al-substituted goethite (and/or hematite), kaolinite, and quartz. Gesso-type yellow and red earths are composed of goethite and/or hematite accompanied by gypsum, anhydrite, and clay minerals. These earths were probably of evaporitic origin. Dark earths are goethite-based pigments, probably originating from the weathering of iron minerals such as iron sulfides, whereas green earths contain iron silicates such as glauconite and celadonite. Finally, several pigments such as Venetian red are manufactured materials [137].

Earths are therefore multicomponent materials that contain not only iron oxides, but also a variety of minerals—namely, kaolinite, quartz, gypsum, anhydrite, and calcite, among others. The hue of ochres and raws is due to the absorption associated with the charge transfer between the ligand (OH^- and O^{2-}) and the Fe^{3+} ion contained in goethite and/or hematite, and depends significantly on the shape and size distribution of particles [195]. As a result of this complex composition, data analysis in techniques such as XRD and FTIR is made difficult by the coexistence of numerous and strongly overlapping signals due to the different components in the sample.

Figure 3.18 illustrates typical square-wave voltammograms of earth pigments attached to graphite electrodes in contact with 0.10 M HCl. Voltammetric curves can, in principle, be grouped into five morphological types whose "holotypes" are depicted in Fig. 3.18 [139, 174]. These holotypes correspond to: (a) Spanish hematite, (b) French yellow ochre, (c) sienna raw, (d) Italian toast umber, and (e) greenish natural umber [139, 174].

The voltammetric response of hematite-based pigments consists of a main cathodic peak at -0.40 V. For French ochres, peaks at -0.15 and -0.40 V are recorded, while siennas' square-wave voltammograms show overlapping peaks at -0.15 and -0.25 V followed by a shoulder near -0.40 V. For umbers, a well-defined peak at $+0.25$ V precedes a voltammetric profile similar to that of siennas. Finally, for greenish natural umber, the voltammogram is essentially limited to a prominent peak near $+0.25$ V, preceded by a peak at $+0.58$ V. This last can be attributed to the presence of MnO_2—a frequent component of earths, whose electrochemistry has been widely studied and described [113, 128, 171, 196–202]. The observed peak can be described in terms of the reduction process:

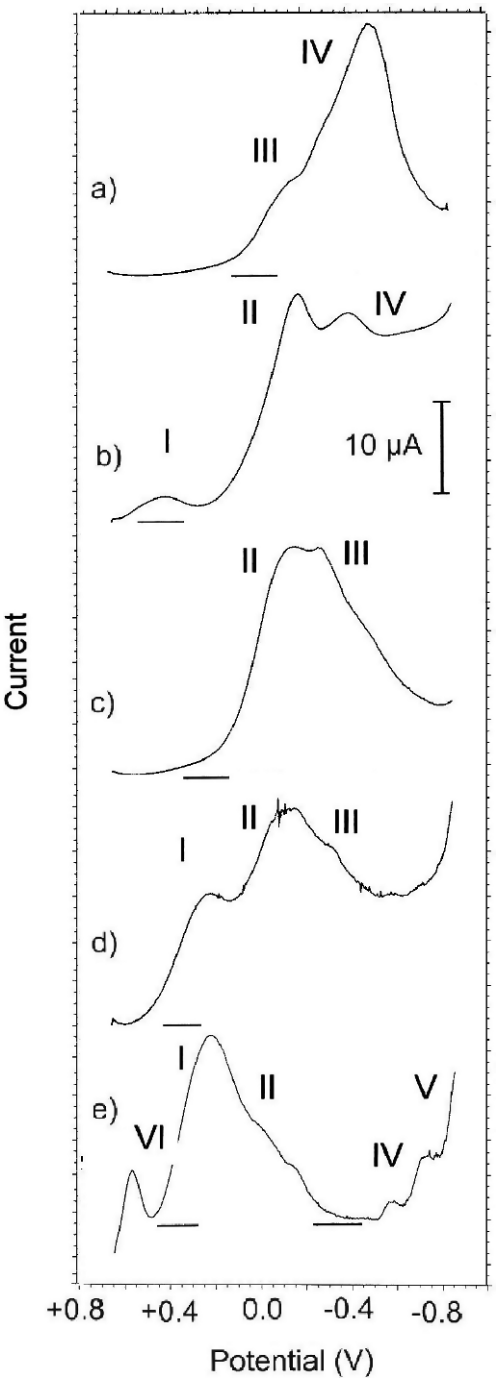

Fig. 3.18 Square-wave voltammograms of PIGEs modified with (**a**) Spanish hematite, (**b**) *yellow French ochre*, (**c**) sienna raw, (**d**) Italian toast umber, and (**e**) *greenish* natural umber immersed in 0.10 M HCl. Potential scan initiated at +0.65 V in the negative direction; potential step increment 4 mV; square wave amplitude 25 mV; frequency 5 Hz [139]

$$MnO_{2s} + H^{+}{}_{aq} + e^{-} \cdots \rightarrow MnO(OH)_{s} \tag{3.20}$$

The electrochemistry of iron(III) oxides, hydroxy-oxides, and related materials has received attention in the last few decades [108, 113, 114, 137–147]. The electrochemical parameters are phase-specific and the kinetics of the electrochemical reaction are affected by the pH and the presence of other chemisorbing ions and/or complexing species. The kinetics of the electrochemical process can be described on the basis of the model developed by Grygar [147, 148]. Accordingly, the rate of reductive dissolution is driven by the detachment, via ion diffusion or complexation reaction, of metal centers from the reduced metal sites in the surface of the solid particles. As a result, the position and shape (roughly, peak width) of the voltammetric peaks depend on the average particle size and the homogeneity of the particle size distribution [147, 148]. Thus, voltammetric peaks are shifted cathodically by increasing Al-for-Fe substitution, increasing particle size, and anodically by increasing departures of stoichiometry—the wider peaks hence indicate less consolidated, and hence probably more heterogenous, iron oxides [137].

Electrochemical identification of earths can be derived from shape-characterizing parameters. Roughly, peaks at $+0.25$ V (I) can be attributed to amorphous, highly hydrated iron oxide forms, whereas peaks at -0.15 V (II) and -0.30 V (III) are attributable to goethite and hematite forms with variable degrees of hydration and crystallinity. Peaks at -0.40 V (IV) can unambiguously be attributed to crystalline hematite forms. For chemometric purposes, normalized peak currents, $I(j)$, for the above peaks (j = I, II, III, IV) were tabulated and included in 2D diagrams. As can be seen in Fig. 3.19, where the $I(II)/I(IV)$ ratio is plotted against the $I(III)/I(IV)$

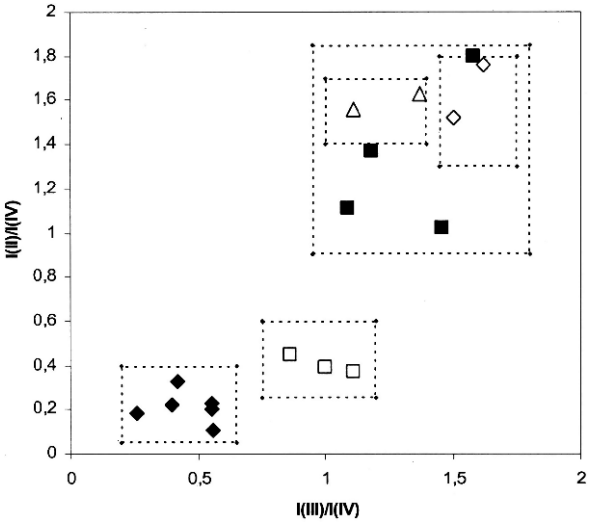

Fig. 3.19 Plot of $I(II)/I(IV)$ vs. for earth pigments differentiating hematite-based (*solid rhombs*), goethite-based clays (*solid squares*), siennas and Spanish ochre (*rhombs*), French ochres (*squares*), and umbers (*triangles*). From square-wave voltammograms of pigment-modified PIGEs immersed into 0.10 M *HCl*. Potential scan initiated at $+0.65$ V in the negative direction; potential step increment 4 mV; square wave amplitude 25 mV; frequency 5 Hz [139]

Table 3.2 Peak current ratios for commercial iron oxide (Fe_2O_3, Aldrich) and earth pigments from Kremer. From square-wave voltammograms of sample-modified PIGEs immersed into 0.10 M *HCl*. Potential step increment 4 mV; square wave amplitude 25 mV; frequency 5 Hz. Adapted from ref. [139]

Pigment	I(I)/I(IV)	I(II)/I(IV)	I(III)/I(IV)	I(VI)/I(IV)
Fe_2O_3FE	0.02	0.20	0.55	0.00
Hematite HE	0.03	0.33	0.42	0.00
Spanish hematite, SE	0.03	0.23	0.55	0.00
Caput mortum, CM	0.03	0.18	0.26	0.00
Venetian red, VR	0.05	0.22	0.40	0.00
Red Bole, RB	0.24	1.37	1.18	0.00
Red Clay, RC	0.76	1.90	1.60	0.00
Goethite GO	0.07	1.11	1.09	0.00
Spanish ochre, SO	0.17	1.02	1.46	0.00
Sienna raw, SR	0.31	1.81	1.62	0.00
Natural Sienna, NS	0.05	1.52	1.50	0.00
Yellow French ochre, YF	0.11	0.37	1.11	0.00
Orange French ochre, OO	0.23	0.39	1.00	0.00
French ochre, FO	0.21	0.45	0.86	0.00
Cyprus umber, CU	0.42	1.56	1.11	0.12
Italian toast umber, IU	1.00	1.63	1.37	0.14
Greenish natural umber	15.4	8.5	4.2	0.33

ratio, the diagram permits a clear distinction between earths, Spanish ochres, and French ochres [139, 174]. The diagram point for green earth was considerably separated from the above and has not been represented.

To obtain a detailed separation of the different types of pigments, and establish hidden relationships between the different voltammetric types, hierarchical cluster analysis was performed. Applying a Dendrogram building analysis of all data in Table 3.2 is shown in Fig. 3.20a. Here, greenish natural umber (GU) separates clearly from all other pigments (ERT branch) so that a second analysis could be performed for all remaining earths. The result is shown in Fig. 3.20b. Here, earth pigments are divided into two major branches. The first one is subdivided into hematite-based materials (FE, HE, SE hematites, Caput mortum, and Venetian red) and French ochres (FO, YF, OO). The second major branch of earths contains (roughly) goethite-based raw materials (GO, RB, RC), Spanish ochre (SO), siennas (SR, NS), and umbers (IU, CU).

3.6 Speciation

A speciation of particular interest is to detect the presence of species in different oxidation states in the sample. The determination of the presence of two or even more oxidation states of a given species, and eventually their relative quantitation, is a highly important analytical target in a variety of applications. The determination of the $Fe(III)/Fe(II)$ ratio in raw and ceramic materials is probably one of the most

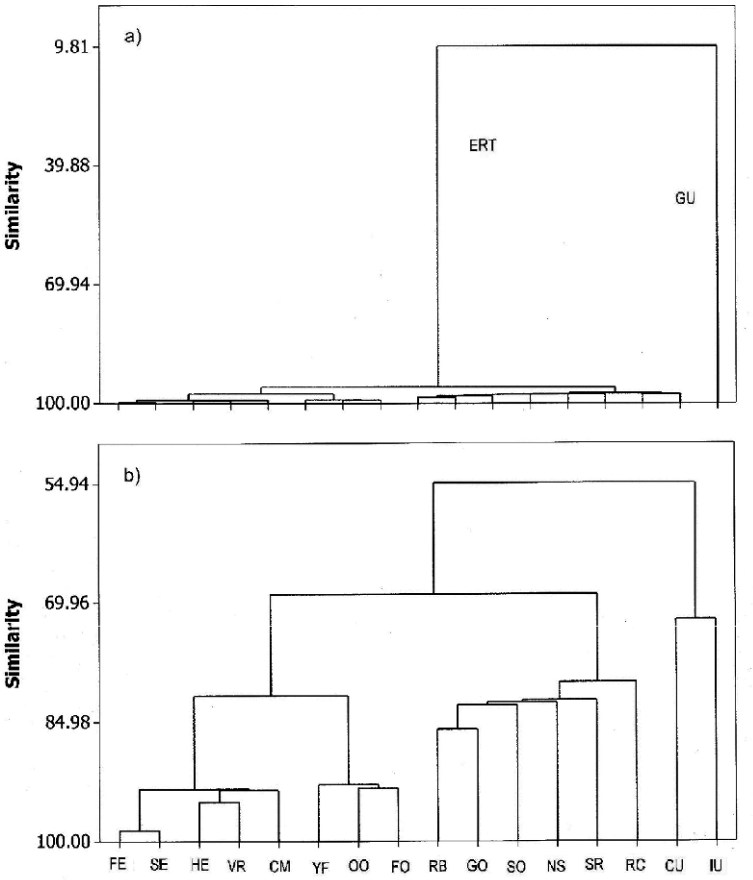

Fig. 3.20 Hierarchical cluster analysis with euclidean distance of the autoscaled variables applied to voltammetric parameters recorded for mineral and pigment specimens studied here. From data in Table 3.2: (**a**) including greenish natural umber; and (**b**) excluding this pigment [139]

paradigmatic examples of this kind of problem. This ratio provides information on the composition of raw materials but also on the nature of thermal treatments used for preparing ceramics.

The general problem of determining the relative amounts of oxidized and reduced forms of an electroactive species in solution was faced theoretically by Scholz and Hermes [203] for the cyclic voltammetry of an electrochemically reversible process controlled by diffusion. These authors used the currents at the larger and lower potential limits (anodic and cathodic switching potentials, $i_{\lambda,c}, i_{\lambda,a}$, respectively) represented in Fig. 3.21. Here, the CV is initiated at -500 mV in the positive direction of potentials, and it is assumed that the diffusion coefficients for the oxidized and reduced forms of the electroactive species (the depolarizer) are identical. Then, the

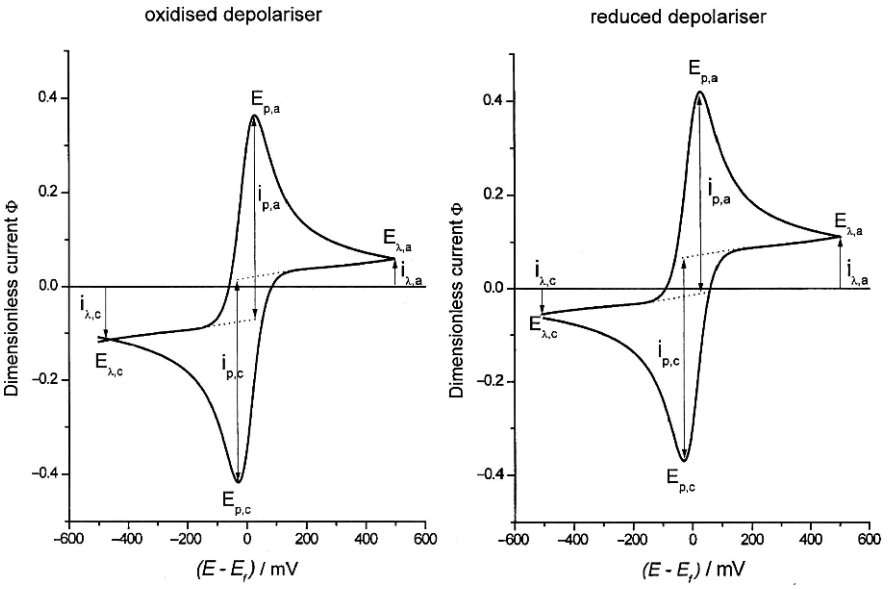

Fig. 3.21 Simulated cyclic voltammograms (2nd cycle) of an electrochemically reversible system with the depolarizer in the bulk of the solution that is in its reduced and oxidized forms, respectively taking: $E_{start} = E_{\lambda,c} = -500\,\text{mV}$, $D_{ox} = D_{rd}10^{-5}\,\text{cm}^2/\text{s}$, scan rate 0.1 V/s [203]

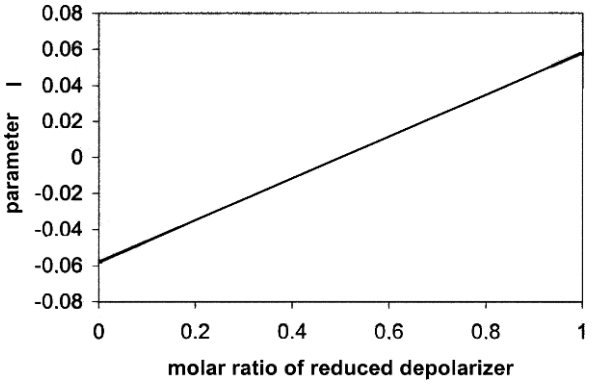

Fig. 3.22 Dependence of the I parameter on the molar ratio of the reduced depolarizer using simulated CVs in Fig. 3.21 [203]

parameter $I = |i_{\lambda,c}| - - |i_{\lambda,a}|$ varies linearly with the molar ratio of the reduced (or oxidized) form. That variation can be seen in Fig. 3.22.

A second procedure has also been proposed [204, 205]. This is based on the measurement of the peak currents for the anodic peak recorded in the first ($i_{pa}{}^*$) and the second (i_{pa}) scans when the voltammogram is initiated at the formal electrode potential of the couple in the positive direction of potentials, as illustrated

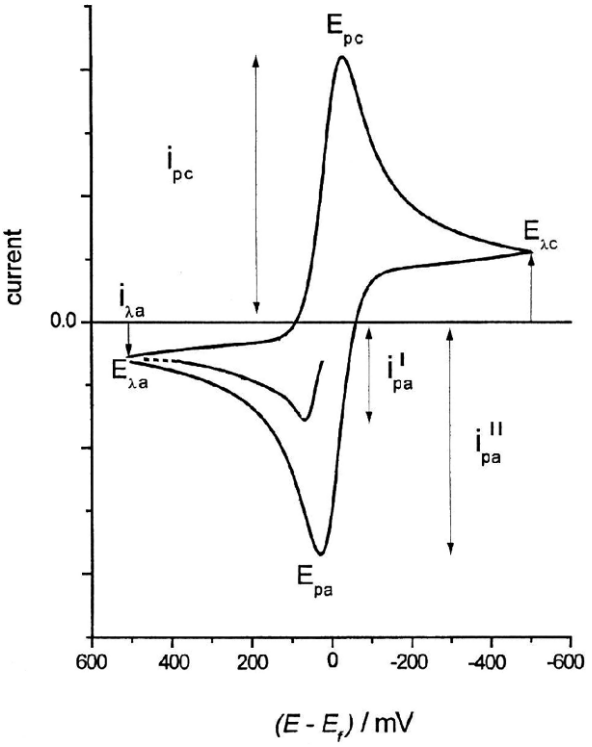

Fig. 3.23 Simulated cyclic voltammograms (1st and 2nd cycle) of an electrochemically reversible system with the depolarizer in the bulk of the solution in its reduced and oxidized forms, respectively taking: $E_{start} = E_{\lambda,c} = -500\,\text{mV}$, $D_{ox} = D_{rd}$ $10^{-5}\,\text{cm}^2/\text{s}$, scan rate 0.1 V/s. The potential scan is initiated at the formal electrode potential of that couple in the anodic direction. Adapted from [203]

in Fig. 3.23. Equivalently, cathodic peak currents can be used. The idea is that on initiating the potential scan for a reversible couple in the anodic direction, if the electroactive species is initially in its oxidized state, an anodic current initially flows so that $i_{pa}{}^*$ and i_{pa} will be similar. On the contrary, if the electroactive species is initially in its reduced form, the initial current will be cathodic, rapidly changing to anodic upon scanning the potential in the positive direction. As a result, the peak current recorded in the first scan will be significantly lower than that measured in the second and subsequent scans.

As a result, the values of the $(i_{pa}{}^*/i_{pa})$ ratio vary systematically with the potential scan rate and the molar fraction of reduced (or oxidized) form in the bulk of the solution. Pertinent data are shown in Fig. 3.24.

The use of these methods for speciation in solid materials requires that two essential assumptions—electrochemical reversibility and diffusive control—apply. Under these circumstances, theoretical CVs for ion-insertion solids are essentially identical to those for species in solution [206]. Since solid-state processes involve coupled

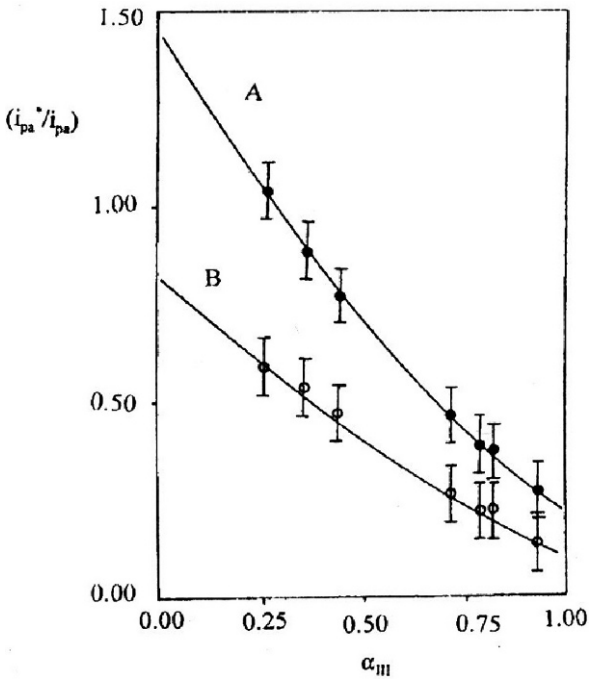

Fig. 3.24 Theoretical variation of the (i_{pa}^*/i_{pa}) ratio with the molar fraction of oxidized form in CVs for a one-electron reversible couple initiated at the formal electrode potential of that couple in the anodic direction for solutions containing different molar fractions of the oxidized form using the base line after (**A**) and before (**B**) the anodic peak [205]

diffusion of electrons and charge-balancing electrolyte ions through the solid, the condition of "ordinary" diffusive control requires relatively concentrated electrolyte solutions [206].

These methods have been applied to the determination of the Fe(III)/Fe(II) ratio in archaeological ceramic materials [205], and are of interest with regard to the so-called Maya Blue problem. Maya Blue is a famous artificial pigment widely used in murals, pottery, and sculptures by the ancient Mayas and other people in Mesoamerica. A typical Maya paint is shown in Fig. 3.25. The pigment hue ranges from bright turquoise to dark greenish blue [207]. A typical wall painting is illustrated in Fig. 3.26. The pigment exhibits a characteristic brightness and a remarkable chemical stability, and is unaffected by the attack of acids, alkalis, oxidants, reducing agents, organic solvents, or biodegradation.

Maya Blue can be described as a hybrid organic-inorganic material resulting from the association of indigo (H_2IN)—a blue dye extracted from *Indigofera suffruticosa* and other plants—with a local clay, palygorskite (known as attapulgite for historians and restorers), which is a fibrous phyllosilicate [207].

The nature of the indigo-palygorskite association, and the reasons for its hue and durability, have become controversial. Shepard [208] first introduced the idea of

Maya Blue as an unusual pigment in a dye attached to certain clays in Yucatan. In 1966, Van Olphen [209] prepared a complex analogous to Maya Blue by heating indigo with palygorskite or sepiolite—both clays with a fibrous structure. Pigments prepared with indigo plus laminar silicates were found not to be resistant to acidic attack. Van Olphen suggested that indigo molecules are too large to enter into the channels of the clay, so such channels are in some way sealed at their ends by indigo molecules [209]. Kleber et al., however, proposed that partial (or even deep) penetration of indigo molecules inside the palygorskite channels is possible [210]. More recently, José-Yacamán et al. [211, 212] proposed that iron and iron oxide nanoparticles in Maya Blue might at least partly account for the observed hue. In contrast, studies performed by Sánchez del Rio et al. [213, 214] did not find either iron in metallic form nor goethite in Maya Blue, in agreement with the idea that the blue coloration of the pigment is originated by the batochromic shift of the indigo absorption bands as a result of the association of the dye to the inorganic support [215–217].

Application of the voltammetry of microparticles techniques to Maya Blue samples, combined with FTIR and UV-VIS spectroscopies, electron microscopy (TEM, SEM/EDX), and atomic force microscopy (AFM) techniques, allowed Doménech et al. [218] to present a novel approach by characterizing the presence of dehydroindigo (the oxidized form of indigo) in Maya Blue [218] and determining thermochemical parameters for the attachment of indigo and dehydroindigo (and leucoindigo, the reduced form of indigo) to the palygorskite matrix [218, 219]. The electrochemical processes for indigo oxidation to dehydroindigo and indigo reduction to leucoindigo are shown in Scheme 3.1. These processes can be clearly recorded for indigo microparticles attached to graphite electrodes, in contact with aqueous electrolytes, as shown in Fig. 3.26a.

The effect of the indigo/dehydroindigo attachment to palygorskite on the Maya Blue hue is illustrated in Fig. 3.27, where the spectra of indigo, dehydroindigo,

Fig. 3.25 Maya blue painting from Calakmul, late classical period. Photograph by M[a] Kuisa Vázquez de Agredos Pascual

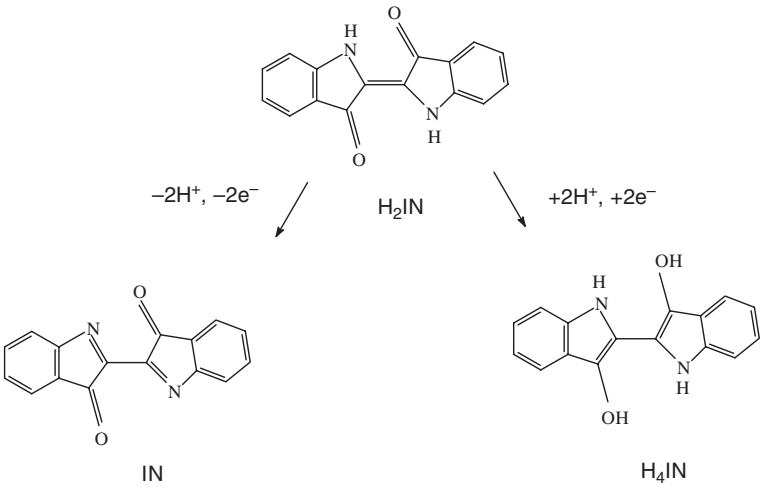

Scheme 3.1 Schematics for the electrochemical oxidation of indigo to dehydroindigo and the electrochemical reduction of indigo to leucoindigo [218]

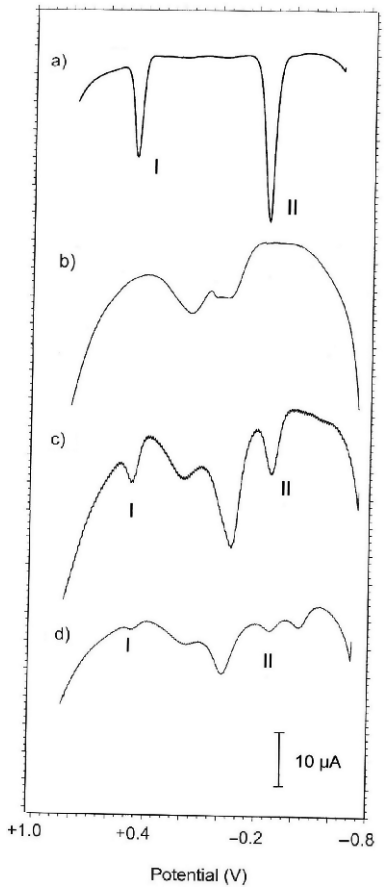

Fig. 3.26 SQWVs of PIGEs modified with (**a**) indigo and (**b**) pristine palygorskite from Sak lu'um, and MB samples from (**c**) Chakmultún, and (**d**) El Tabasqueño, immersed in 0.50 M HAc +0.50 M NaAc buffer at pH 4.85. Potential scan initiated at −750 mV in the positive direction. Potential step increment 4 mV; square-wave amplitude 25 mV; frequency 5 Hz [223]

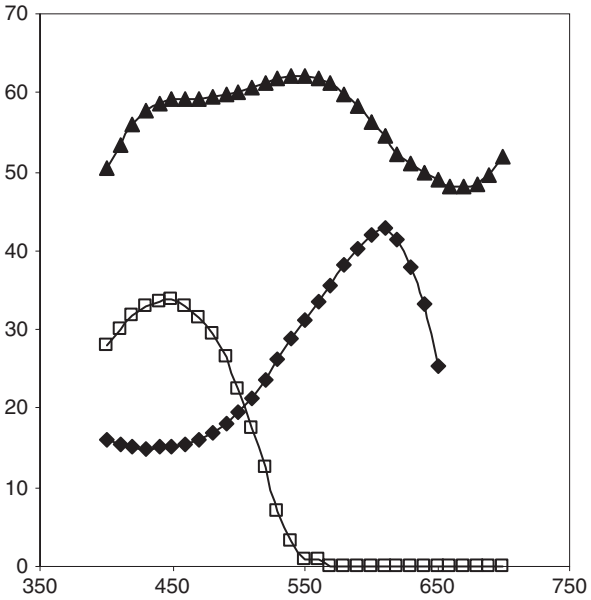

Fig. 3.27 Visible spectra for indigo (*rhombs*), dehydroindigo (*squares*), and a Maya Blue sample (*triangles*) from Calakmul, Late Preclassical period

and a typical Maya Blue samples are superimposed. As studied both theoretically and experimentally by Klessinger and Lüttke [220], indigo exhibits an absorption band with a maximum typically located at 605 nm, while dehydroindigo yields an absorption band with maximum at 425 nm resulting, respectively, in blue and yellow colorations. Spectra of Maya Blue samples produced a two-peak spectrum with maxima located at 440 and 570 nm, consistent with the blue-green coloration of the pigment.

Speciation techniques previously described allowed for estimating the mean dehydroindigo/indigo ratio in Maya Blue samples, as well as its variation with the depth in palygorskite crystals [221]. A maximum dehydroindigo proportion of 25–30% can be established from electrochemical measurements [221].

Application of chemometric techniques to Maya Blue samples from different archaeological sites in Yucatán and Campeche (Mexico) led to propose that different preparation procedures of the pigment were used by the ancient Mayas, the recipes evolving in a ramified form [222]. Reproduction of ancient procedures for preparing indigo specimens from leaves of *Indigofera suffruticosa* [223] also suggested an evolution over time of preparation methods. Additionally, electrochemical data denoted the presence of the pigment in samples from wall paintings in the substructure II-C from the archaeological site of Calakmul, dated in the Late Preclassical period [218]—by far the most ancient sample of Maya Blue currently known.